Low energy π^+ scattering from light nuclei

S. A. Dytman, J. F. Amann,* P. D. Barnes, J. N. Craig,† K. G. R. Doss, R. A. Eisenstein, J. D. Sherman,* and W. R. Wharton
Physics Department, Carnegie-Mellon University, Pittsburgh, Pennsylvania 15213

G. R. Burleson and S. L. Verbeck‡
Physics Department, New Mexico State University, Las Cruces, New Mexico 88003

R. J. Peterson
Department of Physics and Astronomy, University of Colorado, Boulder, Colorado 80309

H. A. Thiessen
Los Alamos Meson Physics Facility, Los Alamos Scientific Labs, Los Alamos, New Mexico 87545
(Received 12 June 1978)

Angular distributions for elastic and inelastic scattering of ~ 50 MeV π^+ projectiles from targets of ^{12}C, ^{16}O, Si, and Fe are reported. Systematic differences between the experimental results and predictions of some first-order theories constructed from free π-N amplitudes are observed for all cases studied. These discrepancies are similar to those reported earlier. Although several improved optical models exist which take into account better treatments of the first-order potential as well as some second-order effects such as π absorption and the Lorentz-Lorentz effect, good agreement with the data cannot be achieved without a phenomenological adjustment of the potential parameters. A purely phenomenological Kisslinger potential when used to fit the data yields potential parameters which are independent of mass number over the A region studied. The resulting p-wave parameter b_1 is close to the value predicted from free πN models, while the s-wave parameter b_0 requires severe adjustment of both real and imaginary parts from the value predicted from free πN models. The inelastic results are compared to distorted-wave Born-approximation calculations, which are seen to manifest characteristics similar to those seen in the elastic channel. A common optical potential is found to provide a good description of both elastic and inelastic scattering.

[NUCLEAR REACTIONS Elastic and inelastic scattering of 50 MeV π^+ from ^{12}C, ^{16}O, Si and Fe. Angular distributions: $25° < \Theta_L < 145°$. Optical model and DWBA of cross-section data.]

I. INTRODUCTION

Low-energy π-nucleus scattering is of considerable importance to the study of π-nucleus interactions. In the low energy region the (3, 3) resonance is not as dominant as it is for scattering processes when $T_\pi \sim 120$–250 MeV. This means that the low-energy pion can penetrate into the nuclear interior rather than be completely absorbed in the surface region. For $T_\pi \sim 50$ MeV the π mean free path is ~ 5 fm rather than ~ 0.5 fm at $T_\pi \sim 180$ MeV. Accordingly, the π becomes a probe of the properties of nuclear matter rather than simply of the nuclear surface.

It has been known for some time[1] that simple optical models of quite different physical origin work rather well in describing elastic data in the resonance region. The Glauber model,[2] which is a high-energy approximation, and the Kisslinger model,[3] designed for low energies, enjoy this success because the (3, 3) resonance dominates other effects. Both models reproduce the qualitative features of the data in spite of the fact that the only input to the calculation is nuclear size and free πN scattering information. Nuclear structure information, such as nucleon binding, Fermi motion, Pauli effects, and short-range correlations are omitted from the simple calculations.

It can be persuasively argued that significant new information about pion propagation in the interior of finite nuclear matter might be obtained by a study of pion induced reactions at low energies. Of these, the simplest are elastic and inelastic scattering processes, where nuclear structure effects of interest can be seen via necessary modifications to first-order potential scattering theories. Pionic atom experiments also probe the pion-nucleus interaction far from resonance and may also be expected to yield information not only about the π-nucleus potential but also about the nuclear periphery, regarding which comparatively little is known. It is hoped that a consistent picture of π-nucleus physics from the subthreshold region through the πN resonances will emerge.

In what follows, we describe experiments on elastic and inelastic scattering using 50 MeV π^+ projectiles on light and medium mass targets. Thus, the first part of a study of the A dependence

of these reactions is completed. In Sec. II a description of the experimental technique is given, while Sec. III contains a comparison of the data to existing theories. A phenomenological analysis is also presented. Section IV contains a summary and conclusions are drawn from this work.

II. EXPERIMENTAL DETAILS

A. Experimental overview

Most of these data were taken on the EPICS beam line[5] at the Clinton P. Anderson Meson Physics Facility. The beam spot at this location has dimensions of 7 cm width and 20 cm height, with the beam dispersed linearly in momentum (±1% of the central value) in the vertical direction. Thus, our measured cross sections are averaged over 1.8 MeV due to beam dispersion. The detector also averaged over ±3° at each angular setting due to the large horizontal beam size and multiple scattering in the targets. No attempt was made to correct for either energy or angle averaging since such corrections (in the kinematic region studied) are generally small. The pion flux measured at the target position was about 5×10^5 pions per second with a primary proton beam of 70 μA. The beam on target was composed of π^+, μ^+, and e^+ in the ratio 1:0.5:0.5.

The pion detection apparatus used in the EPICS runs is shown diagrammatically in Fig. 1. The heart of the system is the dual crystal intrinsic germanium spectrometer[4] (described below), which is capable of stopping 50 MeV π^+ particles within the second crystal, allowing the use of particle identification techniques for π^+-μ^+ separation. The energy resolution obtained in the pion spectrometer ranged between 600 and 1500 keV after correcting for beam dispersion and is largely target-related. The large beam spot also necessitated the use of three helical delay-line proportional chambers (see below) to obtain trajectories of all detected particles for the purpose of energy and angle definition. The scintillators surrounding the Ge detector allowed detection of outscattered nonstopping particles. The distance from target to front Ge crystal was 60 cm, providing a solid angle of approximately 2.4 msr. Beam intensity was monitored using two ion chambers positioned 1.2 m downstream of the target.

The data for the ^{12}C 0$^+$ state at 7.65 MeV excitation, and the 3$^-$ state at 9.64 MeV (forward of 110°) were accumulated on the LEP channel[5] at LAMPF using basically the same detector geometry. However, an 8-crystal Ge detector[4] was used, in which the 50 MeV π^+ projectiles stop in the fourth crystal. Different wire chambers and ion chambers

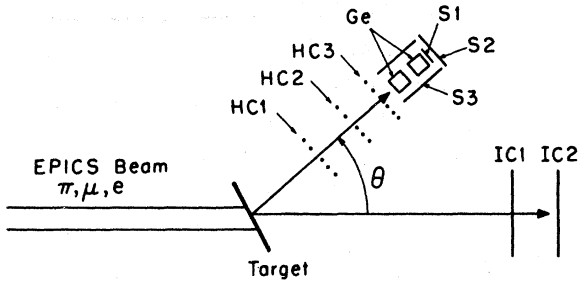

FIG. 1. A schematic diagram of the experimental apparatus. When the incident π passes through the target and scatters through angle θ, it then passes through three delay-line readout proportional chambers (HC1, 2, 3) and into the dual crystal intrinsic Ge detector. Scintillators S1, 2, 3 detect particles which scatter out or pass through the detector and cover 4 out of 5 exits. Ion chambers IC1 and IC2 monitor the incoming beam flux. See text for more details.

were used also. The two data sets were normalized via comparison of the ^{12}C elastic cross sections.

B. Ge spectrometer and wire planes

The Ge spectrometer is composed of two Ge crystal cylinders of diameter ~3.3 cm and thickness ~1.3 cm. Except for thin electrical contacts on the front and back faces, the entire volume of each crystal is sensitive to ionization by incoming particles. A Ge stack of this thickness will stop a pion of 48 MeV kinetic energy. Although the intrinsic energy resolution of this device should be about 40 keV for 50 MeV pions, it was not realized in practice due to contributions from the beam (60 keV), the target, and from straggling in air, various windows and the detector electrical contact (~175 keV). Using a thin Pb target, an energy resolution of 450 keV full width at half maximum (FWHM) was measured in a scattering geometry in order to determine an experimental lower limit on the resolution and a measure of the elastic peak shape (see Fig. 2). The resolution is of course degraded when thicker targets are used.

Dividing the detected particle's energy loss between two crystals allows the use of conventional range-energy particle identification (PID) techniques.[6] A PID number is calculated from the individual energy losses ($E1, E2$) in each crystal:

$$\mathrm{PID}=10[(E_1+E_2)^{1.73}-(E_2)^{1.73}]^{1/2}.$$

Figure 3 is a sample histogram of events classified according to PID. All such events originate in the target and stop in the second crystal. The peaks are formed by particles which lose all their energy by ionization. Particles which scatter out of the detector, or that lose energy by a nuclear

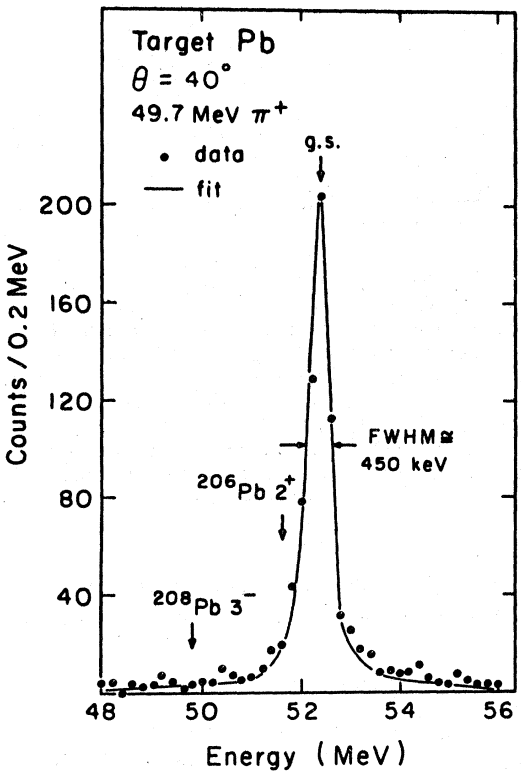

FIG. 2. The elastic scattering peak observed for 50 MeV π^+ scattering from a Pb target at $\theta = 40°$. Target thickness was 290 mg/cm^2 and is the largest contributor to the resolution. The solid curve is the best-fit peak shape as described in the text; the normalized χ^2 is 0.84. The data have been corrected for the dispersion of the incident beam.

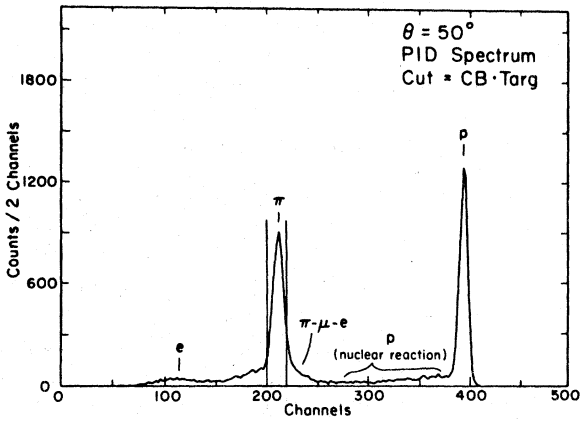

FIG. 3. A particle identification (PID) spectrum obtained using the $\Delta E - E$ technique described in the text. To obtain this spectrum, detected particles must originate from the target (target cut) and stop in the detector (*CB* cut). The detailed peak shapes are discussed in the text. The PID window used for the pion cut in determining final spectra is indicated by the vertical lines.

reaction with a germanium nucleus, fall into the (low PID) peak tails. Events on the high PID side of the pion peak are pions that have given up more than their kinetic energy through decays.

More than 99.9% of the pions decay via $\pi^+ \rightarrow \mu^+ + \bar{\nu}$ and the muons subsequently by $\mu^+ \rightarrow e^+ + \nu\bar{\nu}$, with mean lifetimes of 26 ns and 2.2 μs, respectively. Any energy given up by the decay products during the effective linear amplifier integration time (~0.5 μs) will be collected. Within that time almost all pions will have decayed, and the decay muon will have deposited its 4.1 MeV kinetic energy in the crystal. Essentially all stopping pions will therefore produce an additional (constant) 4.1 MeV in addition to their kinetic energy. This additional energy deposit will not affect the energy resolution. However, the decay electron will have between 0 and 53 MeV kinetic energy, generally giving up 0–10 MeV in the crystal. These electrons produce the tail on the high side of the pion peak in Fig. 2. This tail includes ~15% of all stopping pion events. The vertical lines in the figure show where the PID cut was made during final data analysis.

To tag events in which the particle did not stop in either detector because of scattering out the sides or passing through the rear, scintillators S1 and S2 covered four of the five sides. For each scintillator firing, a bit was set in a coincidence buffer and logged on tape with other event information.

Three helical-decay-line-readout wire chambers[7] were placed between the detector and the target in order to plot straight-line trajectories for all detected particles. Spatial resolution for projecting to the target was measured as 0.6 cm in the vertical direction and 1.2 cm in the horizontal direction. These were measured using a grid of small diameter (0.2 cm) wires as a target.

In addition to providing a correction to measured energies to account for beam dispersion, the chambers cut out all events not projecting to the target. At low π energies and forward angles, this is a significant correction because the short π lifetime provides an abundance of nontarget-related background. For 50 MeV π, the decay rate of the beam is about 11%/m, producing μ^+ of up to 71 MeV kinetic energy. Phase space limits the μ^+ to a cone of opening angle $\theta \leq 18°$. However, owing to decays upstream of the target, the detection apparatus sees a very high flux of spurious particles with energy loss characteristics very similar to the scattered pions of interest. Therefore, shielding is crucial if the singles count rates are to remain tolerable. At angles $\theta > 30°$, the shielding plus target projection and PID cuts reduce the non-

target-related background to that arising from scattering from the air in the vicinity of the target. This source is less than 1% of the normal elastic peak height. For $\theta \leq 30°$, a significant number of decay μ^+ from the upstream side of the target can pass, with good geometry, inside the shielding and enter Ge1. For the 25° and 30° runs, a correction of a few percent was made to account for muons misidentified as pions. For $\theta \leq 18°$, the decay μ^+ pass through the target and the target cut cannot distinguish pions from muons. Figure 4 shows, for a run at $\theta = 25°$, the energy spectrum obtained before and after cuts for PID, π outscattering (CB), and target position were made. Without these cuts the analysis of these data at this angle would have been almost impossible.

The total energy spectrum for all events taped in a typical run (^{12}C at $\theta = 50°$) is shown in the upper half of Fig. 5. After all cuts are made, the spectrum in the lower half of Fig. 5 results. The situation is greatly improved from the 25° run because the scattering angle is larger.

During the runs complete information for all events satisfying a fast coincidence requirement between the two Ge crystals was recorded on magnetic tape for later analysis.

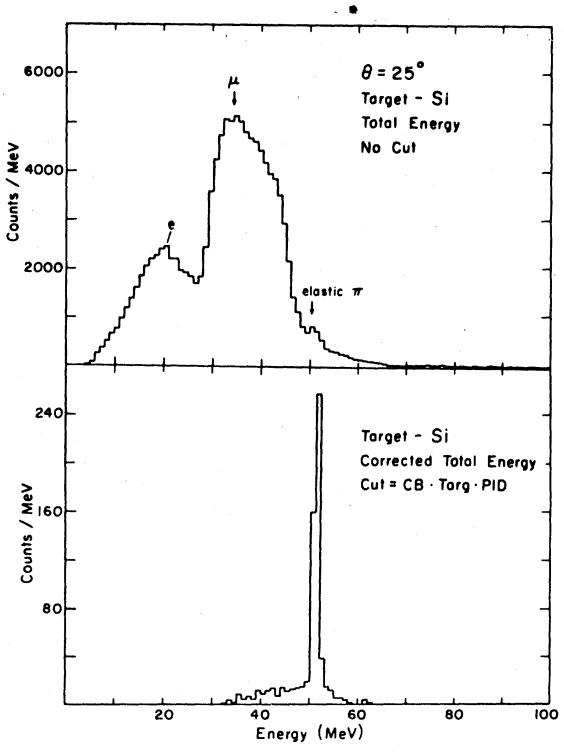

FIG. 4. Two plots of particle number vs total energy obtained for $\theta = 25°$. In the top graph, the π elastic peak of interest is submerged in background due to electrons, outscattered pions and muons. No cuts have been applied. In the bottom graph, cuts have been applied to ensure that particles come from the target, do not outscatter, and have the proper PID for a pion. The spectrum has also been corrected for beam dispersion.

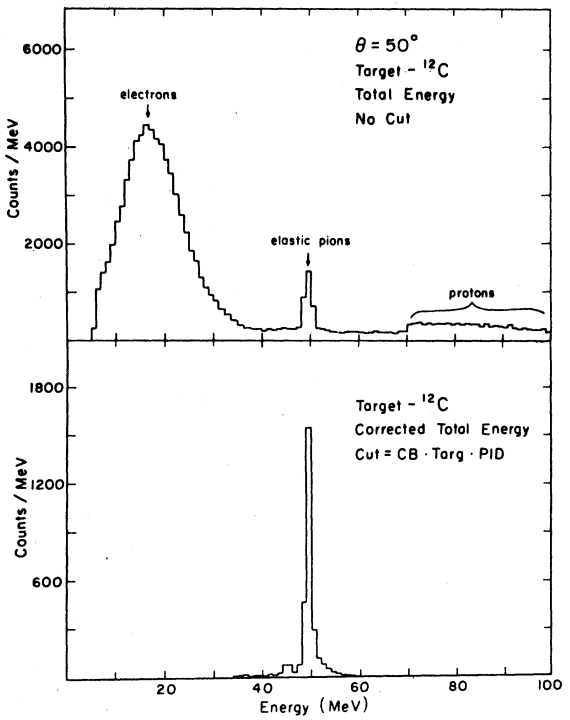

FIG. 5. Same as Fig. 4 but for $\theta = 50°$. Backgrounds are much more tolerable than at $\theta = 25°$, but the cuts again make dramatic improvement in the spectrum.

C. Normalization and monitoring

Two ion chambers about 1.2 m downstream from the target counted the beam particles and provided angle-to-angle normalization once calibrated. Multiple scattering in the target caused some of the beam to miss the front ion chamber, requiring a small (1–2%) correction which was estimated using Monte Carlo techniques. In the case of the 1.2 g/cm^2 water target, a 3% correction was applied.

The absolute normalization for the experiment was fixed by measuring 50 MeV π^+ scattering from the hydrogen in a CH_2 target and comparing to the known values[8] for these cross sections. This determined the product (k) of all angle independent constants, including detector solid angle, detector efficiency, and ion chamber calibration.

The scattering angles for the normalization runs were chosen so that the scattered pion would stop in the second crystal, just as in the data runs, to ensure reasonably constant detection efficiency. Because of this, the normalization runs were all taken at $\theta \leq 75°$. The most forward angle was re-

stricted to $\theta \geq 30°$ in order to separate the carbon and hydrogen peaks. Individual values for k were obtained from 10 different runs (8 using CH_2 and 2 using H_2O) which were then averaged to obtain the final normalization. From the variation in k in these runs the error in k was estimated to be $\pm 15\%$, including the quoted errors for the π^+p cross sections of about 8%. Since all of the data are normalized to the same number, there is no systematic error in comparing different angular distributions.

Since the normalization runs involve pions with energy between 35.0 and 43.7 MeV, the question of the detector efficiency as a function of energy becomes an important one. From an independent measurement and Monte Carlo calculations, the detection efficiency for pions of energy between 35.0 and 48.5 MeV is believed to be constant within ~5%. (The measurement was made by determining the same cross section with varying thicknesses of absorber in front of the detector.) No correction for efficiency change was made for any of the data except for the 120° ^{12}C (3^-) cross section measurement, for which the correction was 10%.

Using the measured absolute normalization constant k, the "equivalent" π^+p cross sections for this experiment can be calculated. These are shown in Fig. 6 together with the phase shift calculation[9] for the incident energy of this experiment and the latest data[8] at 51.5 MeV. There are no systematic deviations with the angle, indicating that effects that change with angle are being treated correctly.

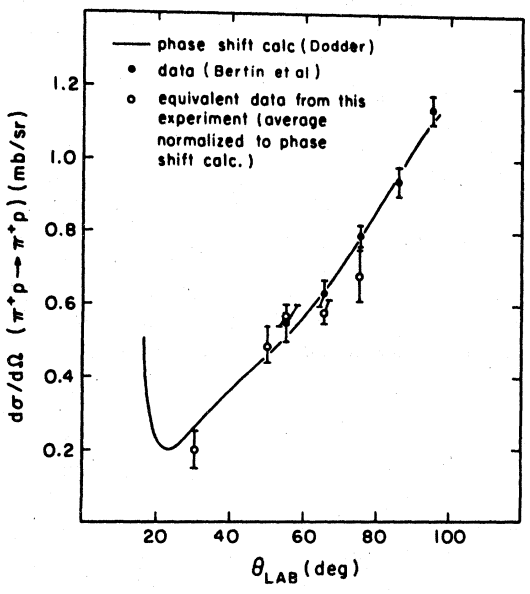

FIG. 6. The differential elastic cross section for π^+p at $E=48.5$ MeV vs scattering angle. The solid circles are the data of Ref. 8 and the solid line is the phase shift fit result of Ref. 9. The open circles are the "results" of this experiment which determine overall normalization of measurements.

D. Reduction of data to cross sections

Peak areas were generally determined by a linear least-squares fitting process. This was because of the complex detector response and the overlap of peaks of interest in several cases. However, the fitting procedure was checked for consistency by a hand subtraction technique.

The pion peak shape for scattering from all targets except hydrogen should differ only in the amount of energy loss and straggling in the target. In each fitting case the peak shape used was an empirical "intrinsic" shape convoluted with a Vavilov[10] straggling distribution. Figure 2 shows the energy spectrum for scattering from Pb and its fitted spectrum. Since the excited states have very few events and the target was thin (290 g/cm^2), this spectrum provides a good test of the intrinsic shape. The amount of straggling width needed to fit each spectrum was proportional to the actual target thickness, although the proportionality constant was empirically adjusted. Spectra for all targets but C and O were successfully fitted with the expected amount of straggling. These discrepancies are not understood at present. The quality of the fits obtained is shown in Fig. 7 where the elastic and two inelastic peaks are simultaneously described by the fitting procedure.

The carbon and iron targets used were constructed from naturally occurring material, and con-

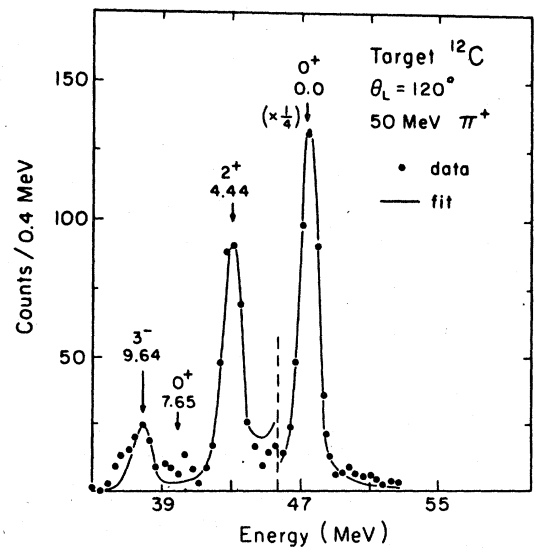

FIG. 7. The computer-generated fit to the energy spectrum obtained at $\theta=120°$ for the ^{12}C target. The elastic and inelastic peaks have been fitted simultaneously. The normalized χ^2 is 1.20.

tained 99% ^{12}C and 92% ^{56}Fe, respectively. Thus impurities corrections were not required. However, in the case of oxygen, a plastic container of water (1.2 g/cm^2) with thin Mylar windows for entrance and exit foils was used as the target. The silicon target was bound using an 8% by weight mixture of Kraton ($CH_{1.4}$) with natural Si. For these targets impurity corrections were made. The energy spectra for events from the carbon and hydrogen contaminations were independently known and fixed during the fitting.

Because of kinematic broadening, the hydrogen peaks had a different shape from those from other targets. In addition, some CH_2 normalization runs had significant overlap of the ^{12}C (2^+) state at 4.44 MeV and the hydrogen peak. Background due to the carbon was independently measured with a carbon target and subtracted from the CH_2 runs. In order to preserve peak shapes, the background ^{12}C run had to be taken with the same target thickness as the CH_2 run. Figure 8 shows the total energy spectrum for the 65° run before and after carbon subtraction. Events in the hydrogen peak are then summed. No background data for the H_2O normalization runs were collected; in these cases the backgrounds were estimated. As this discussion indicates, the hydrogen peak area determination is difficult and results in an increased error for the absolute versus the relative normalization.

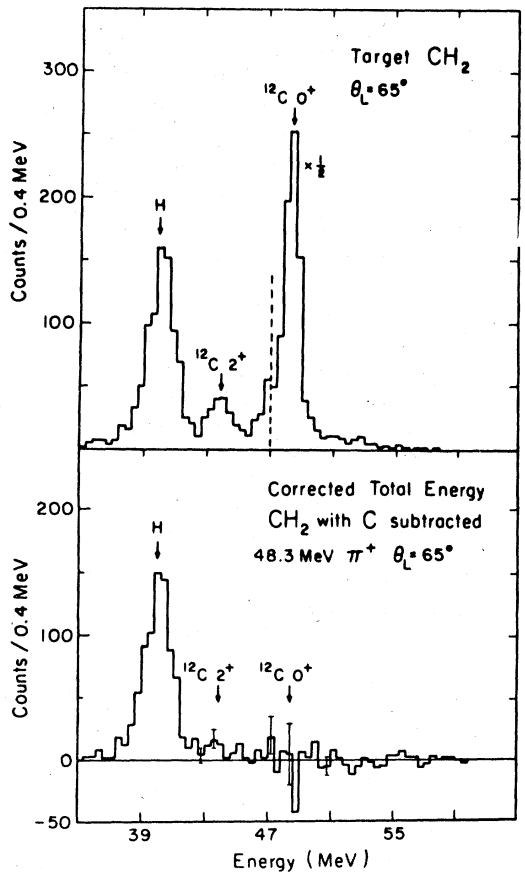

FIG. 8. Energy spectra for the CH_2 normalization runs before (top) and after (bottom) subtraction of the ^{12}C background. See text for details.

As an additional confirmation of the fitting procedure, most of the inelastic areas were also determined by a background subtraction procedure. This was especially important in cases where the computer-generated shape was felt to be inadequate. This procedure involves the subtraction of a "best estimate" background directly from the region of interest in the energy spectrum. The resulting sum of counts is then converted to a cross section.

In some cases, additional corrections were applied to the peak areas. For runs at $\theta = 25°$, about 5% of the peak area was subtracted for decay muons that were not rejected by the target and PID cuts. Finally, from a comparison of fitted with summed areas (see above) for various isolated peaks, *all* fitted areas were increased by 7% to account for a systematically low amplitude in the high-energy tail (π-μ-e events) in the intrinsic shape.

The relative errors include contributions due to statistics, fitting procedure, target thickness variations, and uncertainty in the corrections applied. In addition, a 6% error is added in quadrature to account for germanium detector efficiency variations and changing beam composition (which affects ion chamber calibration).

A good measure of the relative error is to check the reproducibility of the data. In particular, the 35° point for Fe was measured four times under varying conditions, involving change of target thickness, shielding, and beam tuning. Over a span of one month, the standard deviation of the four measurements was 5.5%. In addition, most of the ^{12}C elastic angular distribution was measured twice, once with a full EPICS target, and once as a split EPICS target in a $^{12}C - {}^{13}C$ isotope comparison.[11] In the last case the ^{12}C target covers each half of the beam for an equal amount of time. The cross section variation between these two methods is about 5%, which gives further credence to the above determination.

The final cross sections and errors (in the center-of-mass frame) are given in Tables I–IV. The errors listed are relative errors only.

III. COMPARISONS TO THEORY

A. Qualitative features

The four elastic angular distributions to be discussed are shown in Fig. 9. Shapes range from

TABLE I. A tabulation of the ^{12}C data obtained in the experiment. The scattering angle and cross sections are center-of-mass quantities. The column labeled 0^+ contains ground state cross sections; the label 2^+ denotes the 4.44 MeV state; the label 3^- denotes the 9.64 MeV state; the label 0_2^+ denotes the 7.65 MeV state. The c.m. kinetic energy was 47.11 MeV. The errors quoted are relative errors; the overall normalization is uncertain by ±15%.

	Carbon cross sections $d\sigma/d\Omega$ (mb/sr)			
$\Theta_{c.m.}$ (degrees)	0^+	2^+	3^-	0_2^+
30.9	10.4 ± 0.8	0.34 ± 0.04		0.049 ± 0.014
40.6	7.3 ± 0.5	0.28 ± 0.035		
50.7	4.2 ± 0.3	0.21 ± 0.03		
55.8	3.1 ± 0.2			
60.8	3.0 ± 0.2	0.18 ± 0.025	0.021 ± 0.006	0.025 ± 0.006
65.9	2.9 ± 0.2	0.18 ± 0.025		
75.9	4.0 ± 0.3	0.25 ± 0.025	0.033 ± 0.007	0.023 ± 0.007
91.0	6.1 ± 0.4	0.41 ± 0.05		
100.9	7.5 ± 0.5	0.59 ± 0.06		0.041 ± 0.015
110.9	8.0 ± 0.6	1.1 ± 0.15	0.32 ± 0.04	
120.8	8.6 ± 0.6	1.5 ± 0.2	0.47 ± 0.08	
130.7	6.2 ± 0.6	1.7 ± 0.2	0.60 ± 0.08	
145.5	5.4 ± 0.5	2.4 ± 0.2	0.77 ± 0.10	0.054 ± 0.030

fairly flat (^{12}C) to steeply dropping (^{56}Fe) in a smooth way. For the light elements, the 120° cross sections are comparable to values at about 35°. Each angular distribution has a minimum at 60°–65° that is the dominating feature in carbon but which is barely visible in iron. Forward angle ($\theta \leq 40°$) cross sections increase with Z indicating the influence of Coulomb scattering. At back angles, the structure changes considerably with A. Carbon and oxygen have a broad maximum at ~110°; silicon has a broad small rise at ~90°; with iron, the cross section falls rapidly and a minimum is suggested at ~110°.

Comparisons with existing ^{12}C and ^{16}O data[12-15] are made in Ref. 12. The carbon data to be presented here have been previously reported.[15] When our earliest data[16] are multiplied by a factor of 1.2 to reflect the change in π^+p data[8] in the last three years, the agreement with the new data[15] is excellent at forward angles, but a ~20% discrepancy remains at the more backward angles. The cause is unknown, but the greatly improved detection

TABLE II. A tabulation of the ^{16}O data obtained in the experiment. The scattering angle and cross sections are center-of-mass quantities. The c.m. kinetic energy is 46.77 MeV. The errors quoted are relative errors; the overall normalization is uncertain by ±15%.

Oxygen cross sections	
$\Theta_{c.m.}$ (degrees)	$d\sigma/d\Omega$ (mb/sr)
25.7	15.5 ± 2.5
30.8	12.1 ± 1.5
40.5	7.8 ± 0.7
50.6	5.1 ± 0.5
60.6	3.8 ± 0.3
65.7	4.0 ± 0.3
70.7	4.8 ± 0.4
80.7	5.9 ± 0.5
90.7	7.7 ± 0.7
100.7	8.1 ± 0.7
110.7	8.8 ± 0.8
120.6	7.7 ± 0.8

TABLE III. A tabulation of the Si data obtained in the experiment. All quantities are quoted in the c.m. frame. The c.m. kinetic energy is 48.69 MeV. The mass number was taken as 28.1. The 2^+ state is at 1.78 MeV. The errors quoted are relative errors; the overall normalization is uncertain by ±15%.

	Silicon cross sections $d\sigma/d\Omega$ (mb/sr)	
$\Theta_{c.m.}$ (degrees)	0^+	2^+
25.6	52.0 ± 8.4	
30.6	38.5 ± 9.3	
40.3	25.8 ± 2.1	
50.3	13.2 ± 1.2	
60.4	10.4 ± 1.0	
70.4	10.3 ± 0.9	
80.4	11.7 ± 1.0	
90.4	11.9 ± 1.1	
100.4	10.6 ± 1.0	
110.4	7.4 ± 0.8	
120.4	5.6 ± 0.7	2.6 ± 0.4
130.3	5.1 ± 0.7	1.8 ± 0.7
145.2	4.5 ± 0.5	2.8 ± 0.4

TABLE IV. A tabulation of the Fe data obtained in the experiment. All quantities are quoted in the c.m. frame. The c.m. kinetic energy is 49.29 MeV. The mass number was taken as 55.8. The 2^+ state is at 0.85 MeV and the 3^- at 4.51 MeV. The errors quoted are relative errors; the overall normalization is uncertain by ±15%.

Iron cross sections $d\sigma/d\Omega$ (mb/sr)			
$\Theta_{c.m.}$ (degrees)	0^+	2^+	3^-
25.5	170 ±22		
30.5	118 ±15		
35.3	83 ± 8		
42.1	53 ± 5		
50.1	31 ± 2.6		
55.1	22 ± 2.2		
60.2	17.4 ± 1.6		
65.2	14.0 ± 1.4		
70.2	15.7 ± 1.4		
80.2	10.7 ± 1.3		
90.2	7.4 ± 0.8	1.9 ± 0.5	
100.2	4.4 ± 0.4	2.3 ± 0.4	0.8 ± 0.4
110.2	3.1 ± 0.3	1.7 ± 0.3	1.3 ± 0.4
120.2	4.0 ± 0.4	1.7 ± 0.4	2.4 ± 0.5

technique should make the new data[15] more reliable. The other two data sets are quite close to our new data. Both were taken with scintillators, Ref. 14 normalizing to π^+p scattering as in this work, and Ref. 13 normalizing to the (π^+, pp) reaction which was measured separately. If each data set is weighted equally, the overall normalization error is about ±10%.

Coulomb scattering, for which the analytical form is known, should dominate at small scattering angles. For each nucleus, the data are lower than the Coulomb prediction at 25° and higher elsewhere, indicating that the most forward-angle points of our data are in the Coulomb-nuclear interference region. The Coulomb-dominated region is not covered in our angular range.

As described in Ref. 17, a diffractive minimum should occur at roughly the angle where $qR = 4.4$, the first zero of the spherical Bessel function of order 1. If $R = 1.2A^{1/3}$ fm, this gives an angle of about 95° for iron, 135° for silicon, and unphysical angles for carbon and oxygen. The only possible minimum in our data at back angles is in iron (~110°). However, the general back angle ($\theta \leq 90°$) features of the data seem to follow the diffraction picture. Also, changing the rms radius for iron moves the position of the 110° minimum in calculations. The back angle region will generally be referred to as the diffraction region.

For a pure p-wave optical potential and no "angle transformation",[18,19] there should be a minimum in the angular distribution at 90° within the Born approximation.[17] For the Kisslinger free πN model,[3,20-22] the s-wave parameters are small even at 50 MeV, and the minimum occurs at ~85°. A focus of the calculations[23-26] has been to try to understand why the minimum is shifted forward by an additional 20°. A reasonable "angle transformation,"[18,19] designed to project properly the πN amplitude from the πN to the π nucleus center-of-mass frame, can account for ~10° shift. The remaining shift is probably the result of many competing physical effects, all of which should be included for a proper accounting. In the language of the Kisslinger potential, the position of the minimum is controlled by the values given the s- and p-wave pieces (b_0 and b_1) of the πN t matrix; hence the minimum will be referred to as an s-p interference minimum.[17]

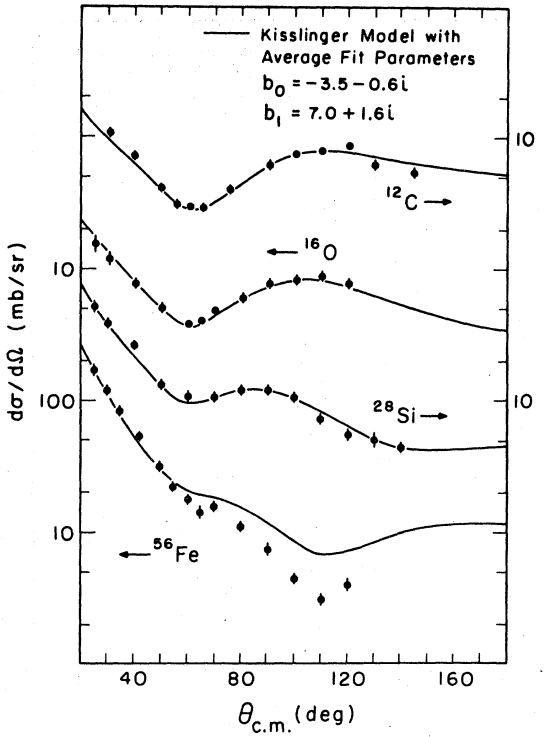

FIG. 9. Angular distribution data for the four targets studied in the experiment. The solid curves are all generated using the average b_0 and b_1 values given on the figure.

The difficulties of the free πN Kisslinger model have been documented previously.[15,18,27-29] Apart from the fact that its quantitative predictions are poor, there are fundamental theoretical objections to the form of the potential. The linear divergence off shell, zero πN range, and the Kisslinger singularity are known problems. In Fig. 10, calculations using this model are compared to the ^{12}C and Fe data. The best results are obtained for the forward angle iron points where the Coulomb interaction is most important. The iron diffraction mini-

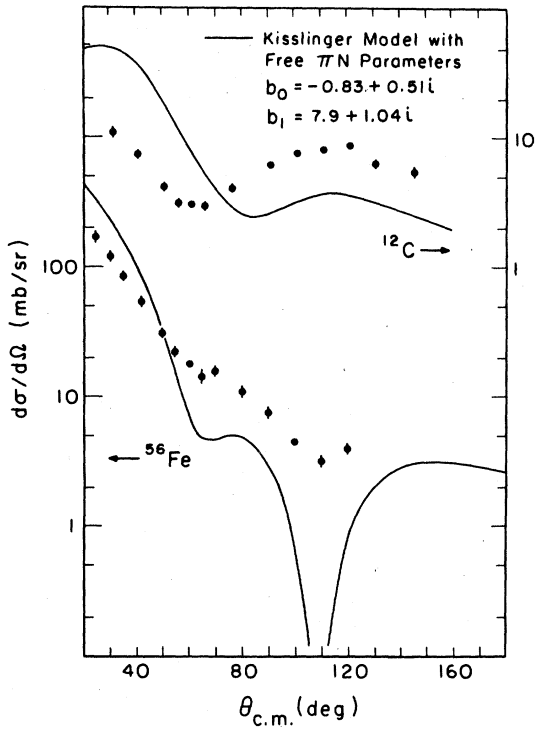

FIG. 10. Angular distribution data for ^{12}C and Fe from this experiment compared to predictions based on the Kisslinger potential generated from free πN information.

mum is in the correct place, but its depth is wrong by almost two orders of magnitude. For carbon, the model prediction is wrong by at least a factor of 2 almost everywhere, due to the diminished influence of Coulomb interactions at small A.

A general indication of the difficulties with this potential can be gleaned from a phenomenological analysis. The computer code FITPI[30] was used to find the best-fit optical model parameters in the Kisslinger potential. The nuclear density parameters are taken from electron scattering analyses[31] and should be known to about ±5%. Each data set was fitted by allowing the complex parameters b_0 and b_1 to vary freely. The nuclear matter density had a p-shell Gaussian shape for ^{12}C and ^{16}O, and a Fermi shape for ^{28}Si and ^{56}Fe; the parameters used are listed in Table V. Resultant fit values for b_0 and b_1 can be found in the same table and in Fig. 11. In all cases an excellent fit is obtained with χ^2/N never exceeding 1.2.

In Fig. 11 the best-fit parameters are displayed as a function of mass number A. The lines in each section represent the b_0 and b_1 theoretical values for a self-conjugate nucleus derived from free πN scattering data.[32] The width between lines represents the spread allowed by the various phase shift sets available. Both the lack of low-energy πN data and a cancellation between the $T=\frac{3}{2}$ and $T=\frac{1}{2}$ s-wave amplitudes increases the uncertainty in b_0.

We note that the fit values of b_1 are relatively close to the free πN prediction, while the fit values of b_0 are drastically different from the prediction. It has been shown by Cooper and Eisenstein[17] that, when using a phenomenological analysis of the Kisslinger type, such excursions of b_0 are necessary if one is to move the minimum position the requisite amount. This is especially true if one assumes that the p-wave resonance is still dominant at these low energies, as it apparently is. Hence, one of the major findings of the phenomenological analysis is a need for a very strongly repulsive s-wave parameter $\mathrm{Re}(b_0)$. This is reminiscent of the situation in pionic atoms, where a similar situation has been noted.[33] We note in passing that some of the improved theoretical treatments yield a stronger s-wave repulsion, after including the angle transformation and the ef-

TABLE V. Fitting results with Kisslinger free πN model. A tabulation of the matter and charge density parameters used in the calculations. Column 4 gives the rms proton radius determined from electron scattering (see Ref. 31); the shape (col. 5) is either a p- shell Gaussian (G) or a Fermi (F) distribution. The parameters for the shape used are given in cols. 6 and 7. The best-fit parameters in the Kisslinger potential which resulted from the χ^2 minimization are given in cols. 9–13. None of the fits except ^{12}C are in violation of unitarity; for this element the inelasticity parameter $\eta_0 = 1.05$, while all other partial waves have $\eta < 1$. A violation of unitarity at this level is probably not statistically significant.

Nucleus	A	Z	$\langle r^2\rangle^{1/2}$ (fm)	Shape	r_0 (chg) (fm)	c or w (fm)	a or α (fm)	$\mathrm{Re}b_0$ (fm^3)	$\mathrm{Im}b_0$ (fm^3)	$\mathrm{Re}b_1$ (fm^3)	$\mathrm{Im}b_1$ (fm^3)	χ^2/N
carbon	12	6	2.46	G	1.36	1.69	1.08	−3.6±.1	−0.63±0.42	7.2±0.1	1.7±0.8	10.1/9
carbon[a]	12	6	2.46	G	1.36	1.69	1.08	−3.8±.1	−0.57±0.46	7.7±0.1	1.5±0.9	12.2/9
oxygen	16	8	2.72	G	1.39	1.83	1.54	−3.6±.1	−0.56±0.21	6.9±0.1	1.5±0.4	2.5/8
silicon	28.1	14	3.15	F	1.34	3.14	.54	−3.5±.1	−0.53±0.11	7.0±0.1	1.7±0.2	3.0/9
iron	55.8	26	3.79	F	1.28	3.97	.59	−3.2±.1	−0.10±0.08	6.9±0.2	1.1±0.1	3.9/10

[a]Data multiplied by 1.15.

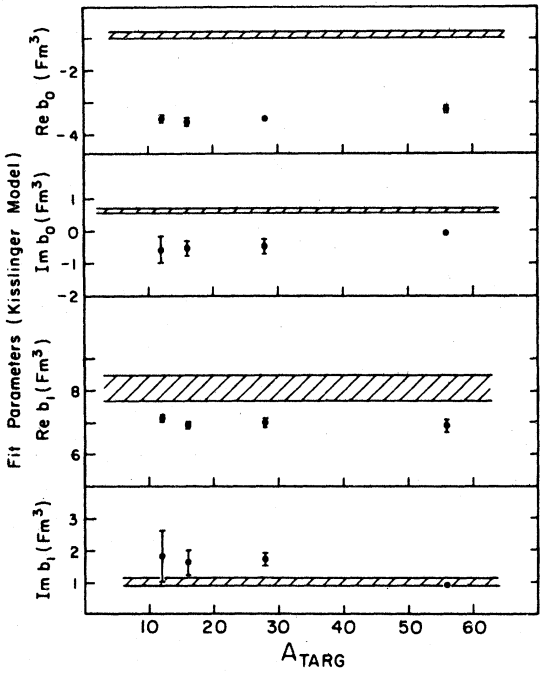

FIG. 11. A comparison of the best-fit (phenomenological) parameters b_0 and b_1 to the predictions of free πN models. The shaded regions represent the spread allowed in each parameter as calculated from the sources in Ref. 32. Note the large excursions required of b_0 compared to those required of b_1.

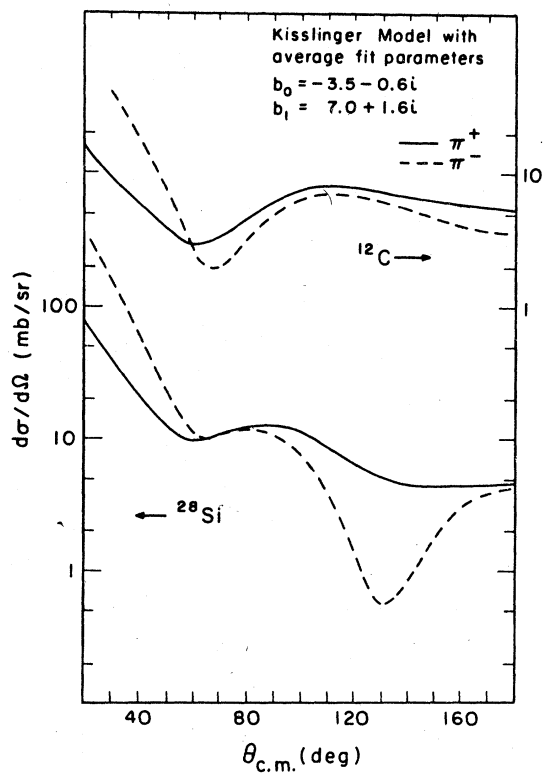

FIG. 12. The predictions of the best-fit phenomenological optical potential for 50 MeV π^- and π^+ scattering from ^{12}C and ^{28}Si.

fects of true pion absorption.

We also note the change in sign of Im(b_0), which is again related to the minimum shift; this sign change *can* lead to unitarity violation but need not do so necessarily since it is the *total* imaginary potential which determines whether violations of this type occur. In the data presented here, unitarity violations occurred in the fits for carbon. These exist only for the π-nucleus s-wave and are small ($\leq 5\%$); they are within the statistical limits on the data.

An examination of the fit values of b_0 and b_1 in Table V shows that in all cases the real values of b_0 and b_1 are determined with high accuracy, while the imaginary parts are less well determined. However, as A increases, the accuracy of the imaginary terms increases; we believe this is due to the onset of diffraction effects as nuclear size increases.

Finally, the fit values plotted in Fig. 11 are seen to be *essentially constant* as a function of mass number A. An important finding of this work, is, therefore, a set of *effective interaction* strengths capable of describing the scattering of 50 MeV π^+ from light nuclei. This is significant since the nuclei studied range from carbon, which is mostly surface, to iron which has a nuclear matter interior. The slight departure from the mean exhibited by the iron fit is quite likely due to the small missing isovector piece not included in the potential. The resulting set of average parameters determined is given in Table V. The average set is used to calculate the scattering for the nuclei studied here; the results are shown in Fig. 9.

Predictions for 50 MeV π^- scattering from ^{12}C and ^{28}Si using the phenomenological optical potential are shown in Fig. 12. The structure of the angular distributions is much more pronounced due to constructive Coulomb-nuclear interference. Comparison of these distributions with data would be of considerable interest.

To test the effect of a possible error in absolute normalization, the ^{12}C data were scaled up by 15% and refitted. The new parameters are different by about 7% and none of the above arguments would be altered.

A somewhat different, though still phenomenological, approach has been taken by Gibbs, Gibson and Stephenson.[34] They use a Kisslinger-type potential, modified to include the effects of finite πN range, the angle transformation, and short-

range correlations. The range is accounted for using a Yukawa form factor with range parameter $\alpha = 500$ MeV/c, while the correlations are included via the Lorentz-Lorentz-Ericson-Ericson (LLEE) prescription involving a correlation parameter ξ. The adjustable parameters ξ, b_0, and b_1 are varied until a best fit to the data of Ref. 13 is achieved. The results are $\xi = 0.21$, $b_0 = -3.62 - 0.02i$, and $b_1 = 7.43 + 1.48i$. The values for b_0 and b_1 are quite close to those obtained here with a substantially simpler potential. Neither model includes true π absorption, which is thought to be quite important at the energies studied here.

B. Quantitative models

Recently, four additional groups[23-26] have published calculations of low-energy pion scattering. All of these calculations use the framework of a multiple scattering series, but with differing emphases. Each attempts to improve on the approximations made in the simple Kisslinger potential model; these improvements are discussed below. At present there are other calculations in progress whose assumptions differ substantially from those of the multiple scattering formulations. These include field theory approaches[35] that emphasize the possibility of pion annihilation or creation in nuclear matter, and resonance dominance models[36] that examine the pion propagation in nuclear matter through its coupling to πN resonances. No results of these calculations are presented here.

1. Momentum space calculations

The principal advantage of momentum space calculations lies in the fact that many higher-order corrections to the simplest first-order theories are most naturally expressed in terms of the kinematic variables of the problem. Direct treatment of the problem in momentum space obviates the need for a complicated Fourier transform of the potential into coordinate space. The chief difficulty is the need to solve an integral equation for each partial wave.

The initial effort in the momentum space method was that of Landau, Phatak, and Tabakin.[18] Improved models are due to Landau and Thomas[23] and Liu and Shakin.[25] The result of their first-order calculations for 50 MeV π^+ scattering from ^{12}C can be found in Fig. 13. These include finite range, angle transformations, Fermi motion, and nuclear binding effects. Nevertheless, the predictions are too low by at least 20% at all angles. At this stage, each calculation includes a careful treatment of first-order effects within multiple scattering theory and has attained similar results which differ considerably from the Kisslinger prediction.

Each calculation also includes true π absorption ($\pi NN \to NN$), parametrized via a ρ^2 dependence. However, Liu and Shakin fit the four parameters (B_0 and C_0) to the data while Landau and Thomas parametrize them from pion absorption data. The Liu-Shakin fits are to ^{12}C and ^{16}O data from Refs. 13–15 and are quite similar to those shown in Fig. 9. Landau and Thomas use a very rough model to determine B_0 and C_0 in order to avoid new parameters, but the resulting predictions do not match well with the data (see Fig. 14). The back angle prediction is too low for each nucleus; presumably the absorption parameters could be changed to fit the data. The calculation matches the data well at forward angles but, while the s-p interference minimum is at ~65° for each nucleus, its depth is overestimated. It is interesting that the full calculation is quite close to the Kisslinger prediction for ^{56}Fe.

2. Coordinate space calculations

Coordinate space calculations have been made by the University of Colorado[24] and the Michigan State University groups.[26] Reference 24 is an extension of earlier work by Thies[37] and includes predominately second-order effects due to true π absorptions, ρ-meson exchange, other short-range correlations (LLEE effect), and many-body effects due to Pauli blocking. The angle transformation is also included, although important first-order effects such as Fermi averaging and binding corrections are omitted. The calculation also assumes fixed nucleons, and no terms higher than

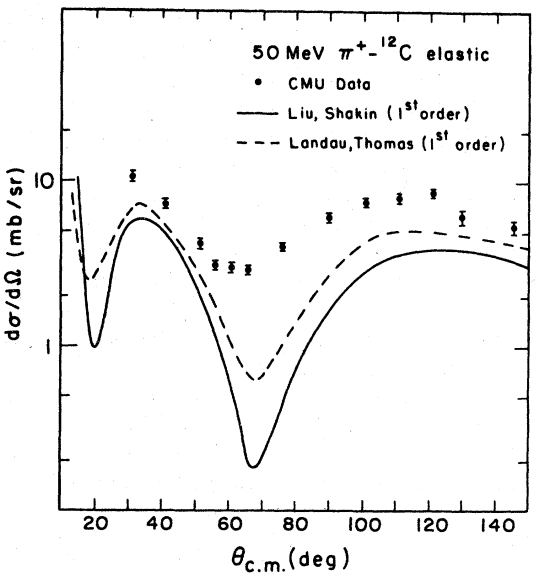

FIG. 13. Comparison of ^{12}C data to the first-order calculations of Refs. 23 and 25.

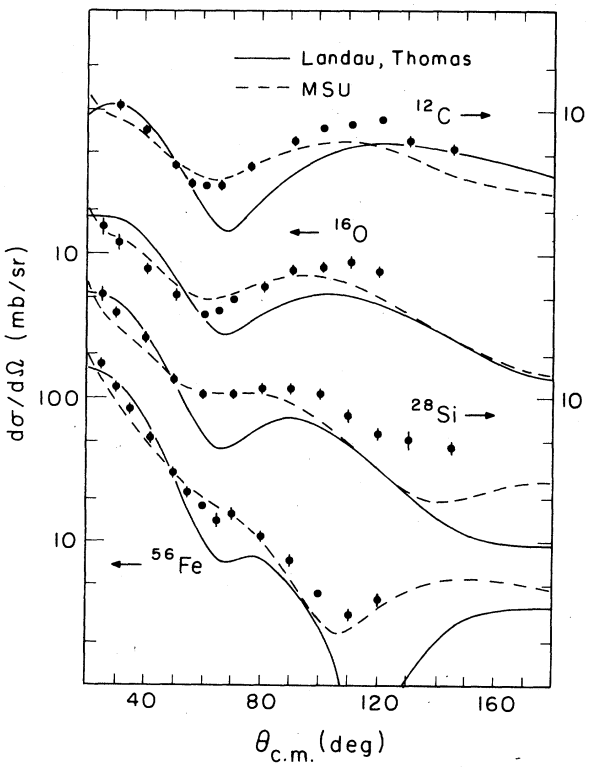

FIG. 14. Comparison of angular distribution data from this experiment to the full calculations of Landau and Thomas (Ref. 23, solid line) and the Michigan State group (Ref. 26, dashed line).

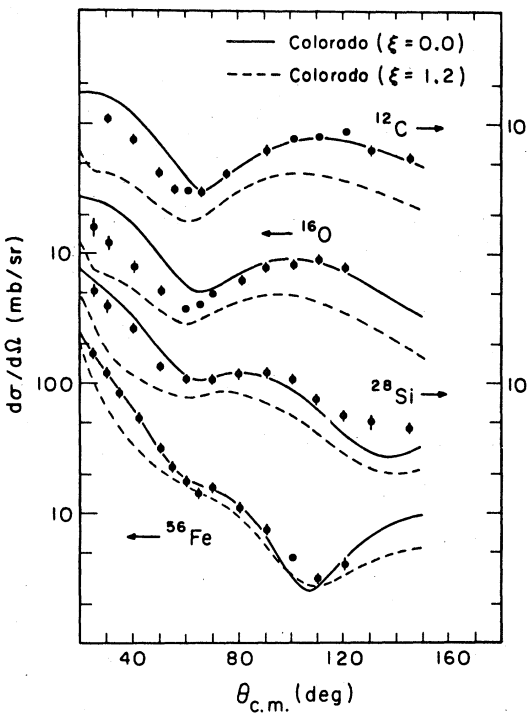

FIG. 15. Comparison of angular distribution data from this experiment to the calculations of Ref. 24. The solid curve ($\xi = 0$) is the calculations with no LLEE effect; the dashed curve ($\xi = 1.2$) represents the full LLEE effect with ρ-meson exchange.

$\rho^2(r)$ are retained. The results of calculations with the LLEE-ρ exchange omitted ($\xi = 0$) and with it at full strength ($\xi = 1.2$) are given in Fig. 15.

It can be seen that the LLEE-ρ effect decreases cross sections in this mass region, especially for carbon. The effect in iron is a small decrease, while in Pb (see Ref. 24) the effect increases the cross section substantially. In addition, the s-p interference minima move from ~65° ($\xi = 0$) to ~60° ($\xi = 1.2$), and diffraction minima move out by ~5°. The calculations involving $\xi = 0$ are much closer to the data than those with $\xi = 1.2$; however, before the LLEE and ρ-exchange mechanisms can be ruled out, a more comprehensive calculation including the important first-order effects should be done.

The calculations done at Michigan State[26] are basically an extension of models used successfully heretofore in π-atom physics. The potential has been modified to include the angle transformation, while most parameters are taken from the analysis of π-atom data. Figure 14 shows the predictions from this potential. The calculations reproduce the trends in the data quite well, although the magnitude at back angles is systematically low. It is encouraging, however, that a reasonable link between pionic atom results and the scattering data at 50 MeV can be established. It should be noted, though, that in order to achieve good agreement with the data, the LLEE strength parameter ξ was raised from the π-atom value of 1.0 to 1.2, and the s-wave repulsion was increased by 30%. In addition, the s-wave π absorption was decreased by 50% from the π-atom value.

From the above discussion it is seen that the theoretical picture of the π-nucleus elastic interaction is still cloudy in spite of rather intensive study on the part of theoreticians. No single calculation has included all of the important, established corrections to the first-order models in a systematic and self-consistent way. Although this is a large task, it clearly needs to be undertaken.

C. Inelastic scattering results

Because of the ambiguities in the elastic analysis described above, it is helpful to appeal to other physical processes for additional information. Other reactions may be sensitive to different parts of the optical potential and further testing would be possible.

During the experimental runs cross sections for scattering to discrete excited nuclear states were also obtained. Since the cross sections are lower and the backgrounds higher, the inelastic data are not of the same high quality as the elastic results. A full angular distribution was obtained[15] for excitation of the 4.4 MeV (2^+) state in ^{12}C, while data for other states (^{12}C: 0^+ at 7.65 MeV, 3^- at 9.64 MeV; ^{28}Si: 2^+ at 1.78 MeV; ^{56}Fe: 2^+ at 0.85 MeV, 3^- at 4.51 MeV) were more limited in angular range. The data are displayed in Figs. 16–18. The data given in Ref. 15 have been adjusted to improve agreement between the computer-generated fits and the hand subtraction analysis (see Sec. II D).

The cross sections for pion excitation of these states can be calculated using a distorted-wave Born-approximation (DWBA) formalism. For this analysis, the code DWPI[38] was used for calculations involving the Kisslinger optical potential; in addition, DWBA calculations were supplied by the Michigan State University group[26] which use the optical potential described above. Transitions to the 0^+ state in ^{12}C were calculated in both DWBA and coupled-channels Born-approximation formalism by Sparrow and Gerace[39] and are described below. In all cases, the deformation parameters β_l were taken from results achieved with other probes. Our calculations involving DWPI ignored the energy difference between incoming and outgoing channels since we lacked a model for the energy dependence of the phenomenological optical potential. The results for each nucleus are discussed in turn.

1. ^{12}C

The qualitative features of the 2^+ angular distribution are a minimum at 65° as in the elastic case, and a fairly flat distribution (see Fig. 16). The figure shows both the elastic and inelastic data; the solid curves are the predictions for scattering from each state using the free πN Kisslinger potential for the elastic scattering and as the distorting potential for the DWBA calculations. Note that the minima thus predicted for the ground and 2^+ states are at ~85°. This is due to the small value

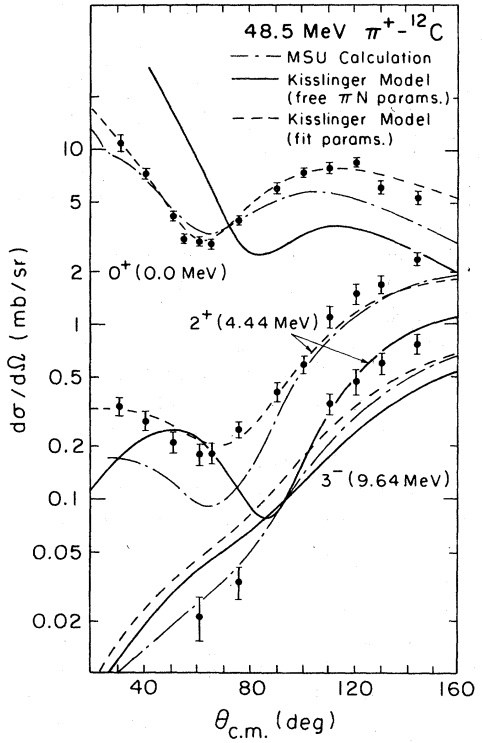

FIG. 16. The ^{12}C angular distribution data of this experiment for elastic scattering and also inelastic scattering to the first 2^+ and 3^- excited states. The solid curves are elastic and inelastic (DWBA) calculations using the Kisslinger potential with free πN parameters. The dashed curves are obtained using the best-fit Kisslinger potential for ^{12}C (see Table V). The dash-dot curves are the calculations from the MSU group (see Ref. 26).

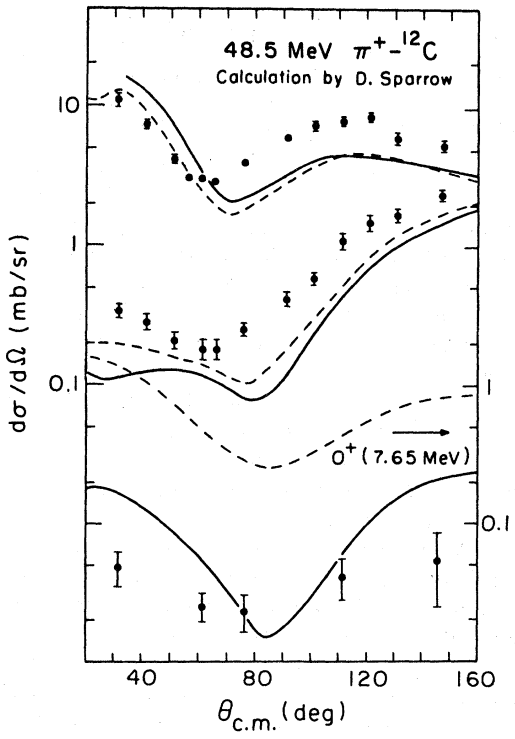

FIG. 17. The elastic and inelastic ^{12}C data from this experiment compared to the calculations of Ref. 39. The solid curves are the coupled-channels calculations described in the text, while the dashed curves are an optical model calculation for the ground state and DWBA calculations for the excited states.

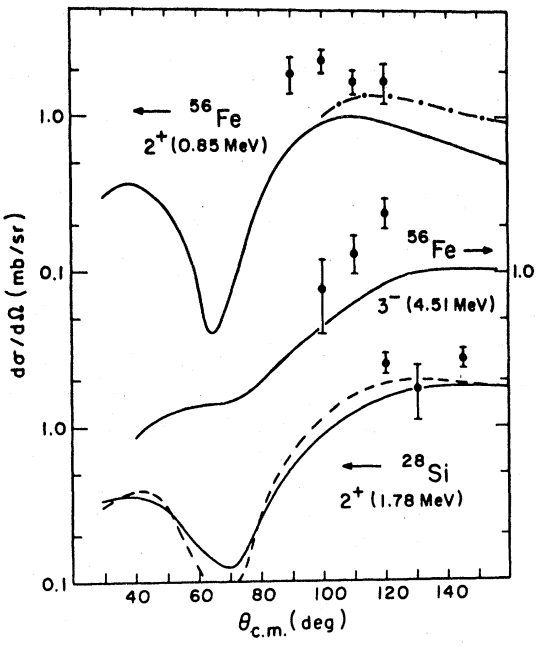

FIG. 18. The Si and Fe inelastic angular distribution data of this experiment compared to the DWBA calculations described in the text. The dot-dash curve for the Fe 2^+ state was calculated using a transition density with a radius parameter 10% larger than the one used for the lower curve. The dashed curve is from Ref. 26.

of b_0 used and to the dominance of the p-wave term involving b_1. The inelastic scattering mirrors the elastic behavior because the piece of the potential responsible for inelastic scattering in DWBA contains the same πN t matrix as does the elastic, viz.,

$$\delta V_{\text{inelastic}} \sim t_{\pi N} \Delta\rho,$$

where $\Delta\rho$ is the difference in nuclear matter density for the excited and ground states. As in the elastic case, the free πN predictions agree poorly with the data.

The situation improves dramatically when the distorting potentials are taken to be the phenomenological ones which best fit the elastic data. Then the inelastic minima and magnitude change so that the predictions become quite good (see the dashed curves in Fig. 16). Similar behavior has been observed at higher energies.[40] The elastic scattering is basically determining $t_{\pi N}$ since $\rho(r)$ is known; thus the inelastic DWBA calculation, insofar as it is valid, can be expected to describe well the inelastic scattering. The DWBA apparently works quite well in this energy region. The β_l values used are $\beta_2 = 0.56$ and $\beta_3 = 0.40$ for the 2^+ and 3^- states, respectively.[41]

Figure 16 shows the results obtained at Michigan State using their "pionic atom" potential to describe the inelastic results. The DWBA calculations for the 2^+ and 3^- states are of about the same quality as the prediction for the elastic scattering.

Figure 17 shows some recent calculations of elastic and inelastic scattering from ^{12}C done by Sparrow and Gerace.[39] Inelastic calculations are made using both DWBA and coupled-channels (CC) formalisms. Channels included are $0_1^+ \rightarrow 0_1^+$, $0_1^+ \rightarrow 2_1^+$, and $0_1^+ \rightarrow 2_1^+ \rightarrow 0_2^+$. For the elastic and 2^+ state, relatively little difference is seen between the CC and DWBA calculations. Again, the agreement between calculation and data for the 2^+ is about of the same quality as the elastic. However, there is an order-of-magnitude disagreement between DWBA and CC for the excitation of the 0_2^+ state at 7.65 MeV. Since the CC formalism takes into account two-step excitations, there is presumably a destructive interference between the one- and two-step amplitudes. The data apparently confirm this interference, as they agree well with the CC calculation. The calculation uses measured transition density information on the 2^+ and 0_2^+ states obtained in electron scattering studies.

2. ^{28}Si and ^{56}Fe

For the other inelastic states measured, the situation is not as clear. Figure 18 shows the data obtained for excitation of the ^{28}Si 2^+ state at 1.78 MeV and the states in ^{56}Fe at 0.85 MeV (2^+) and 4.51 MeV (3^-). DWBA calculations using the code DWPI are also shown; in each case the distorting potential is taken from the best fit to the elastic data and the deformation parameters are taken from other work.[42] A dashed curve represents the Michigan State DWBA result for the ^{28}Si 2^+ state. With such limited angular distributions, cross section magnitudes are all that are being tested here. As far as the calculations are concerned, we find two items of potential interest to further studies. There is fairly large sensitivity to the transition form factor as evidenced by the two curves for Fe, the upper one of which uses a 10% larger radius parameter than the electron scattering value (lower curve). Another interesting feature is the increasing sharpness of the minimum at 65° as A increases, which is opposite to the results for elastic scattering, where the minimum washes out with increasing A.

IV. SUMMARY AND CONCLUSIONS

This paper reports on the scattering of 50 MeV π^+ projectiles from targets of ^{12}C, ^{16}O, Si, and Fe. Angular distributions over the range $25° < \theta_L < 120°$ have been obtained for elastic scattering on all targets; for ^{12}C and Si the most backward angle is 145°. Partial angular distributions for inelastic

scattering to discrete excited states have been obtained for all targets except ^{16}O.

In the case of elastic scattering, systematic differences between the experimental results and the predictions of some first-order models constructed from free πN information have been observed for all cases studied. However, careful treatment of first-order effects such as Fermi motion and the "angle transformation" do much to resolve the disagreement between experiment and theory. Second-order effects due to nucleon binding, short-range correlations (LLEE effect), long-range correlations (Pauli blocking), and true pion absorption all have dramatic effects on the cross-section predictions. With an adjustment of a minimal set of parameters (e.g., those related to true π absorption) some of the second-order theories agree well with the data. It is clear that careful calculations which include simultaneously all such first- and second-order effects should be done.

The elastic data obtained in this experiment have been analyzed phenomenologically using a Kisslinger potential with adjustable parameters b_0 and b_1. One of the principal findings of this work is that these parameters are each independent of A over the mass interval studied. Thus, we have determined an "effective" πN amplitude for nucleons embedded in nuclear matter, which works within the limited confines of this particular model. Only the fit to the Fe data deviates from this simple picture; this is no doubt due to the appearance of isovector effects for this nucleus.

It is also of interest that the phenomenologically determined value for b_1 is much closer to the free πN prediction than is the value determined for b_0. Apparently the resonance is quite pervasive even at these low energies, while b_0 is altered due to the presence of nuclear medium effects and the "angle transformation." Similar findings have been noted in the descriptions of pionic atom data.[33]

Another point of interest is the relative precision with which the real parts of b_0 and b_1 are determined compared to the imaginary. Furthermore, the imaginary parts become better determined as A increases. This may be due to the onset of diffraction effects due to the increase in nuclear size.

Finally, our results for inelastic scattering have been compared to the predictions of DWBA calculations which use both free and phenomenological πN information to calculate the effects of the incoming and outgoing channels *as well as* the transition operator. It is found that optical potentials which fit the elastic scattering well also do quite well in describing the inelastic scattering. In making these calculations, the deformation parameters β_l have been taken from the information obtained using other probes. Thus, the DWBA prescription works well for pion scattering in this energy range and for collective excitations of the type reported here.

ACKNOWLEDGMENTS

We would like to thank the staff of the Clinton P. Anderson Meson Physics Facility for its cooperation in all phases of the experiment. We are especially indebted to Robert Rowher of LASL division *WX*-2 for fabricating the Si targets. The nuclear instrumentation group at Berkeley has helped us greatly in the design, construction, and use of the Ge detector telescopes. We would particularly like to thank Dr. F. Goulding, Dr. R. Pehl, and Dr. A. Thompson for their efforts in this enterprise. Several of our theoretical colleagues have generously communicated their results prior to publication. We would like to thank Dr. R. Landau (Oregon State University and TRIUMF), Dr. K. Stricker (Michigan State University), Dr. G. Stephenson (LASL), and Dr. D. Sparrow (Universities of Colorado and Maryland) for their help in this regard. This work was supported in part by the U. S. Department of Energy.

---

*Present address: Los Alamos Scientific Laboratory, Los Alamos, New Mexico 87545.
†Present address: Science Applications, McClean, Virginia 22101.
‡Present address: W. H. B. Chan and Company, Los Angeles, California.

[1]E. Boschitz, in *Proceedings of the Seventh International Conference on High Energy Physics and Nuclear Structure*, edited by M. P. Locher (Birkhauser, Basel, Switzerland, 1977), p. 133. C. Wilkin, Proceedings of the Spring School on Pion Interactions at Low and Medium Energies CERN Report No. 71-14, 1971 (unpublished).
[2]R. J. Glauber, *Lectures in Theoretical Physics*, edited by W. E. Brittin and L. G. Dunham (Interscience, N. Y., 1959), Vol. 1, p. 315.
[3]L. S. Kisslinger, Phys. Rev. 98, 761 (1955).
[4]J. F. Amann, P. D. Barnes, S. A. Dytman, J. Penkrot, A. C. Thompson, and R. H. Pehl, Nucl. Instrum. Methods 126, 193 (1975). A detailed account of the 8-crystal detector will be included in a forthcoming paper.
[5]Los Alamos Meson Physics Facility User's Handbook.
[6]F. S. Goulding and R. H. Pehl, in *Nuclear Spectroscopy and Reactions*, edited by J. Cerny (Academic, N.Y., 1974), p. 289.
[7]D. M. Lee, S. E. Sobottka, and H. A. Thiessen, Nucl. Instrum. Methods 120, 153 (1974).
[8]P. Y. Bertin, B. Coupat, A. Hivernat, D. B. Isabelle, J. Duclos, A. Gerard, J. Miller, J. Morgenstern, J. Picard, P. Vernin, and R. Powers, Nucl. Phys.

B106, 341 (1976).
[9]D. Dodder, private communication.
[10]P. V. Vavilov, Zh. Eksp. Teor. Fiz. 32, 920 (1957) [Sov. Phys.—JETP 5, 749 (1957)].
[11]S. A. Dytman, J. F. Amann, P. D. Barnes, J. N. Craig, K. G. R. Doss, R. A. Eisenstein, J. D. Sherman, W. R. Wharton, G. R. Burleson, S. L. Verbeck, R. J. Peterson, and H. A. Thiessen, Phys. Rev. C 18, 2316 (1978).
[12]B. M. Preedom, p. 119 of Ref. 1.
[13]D. J. Malbrough, C. W. Darden, R. D. Edge, T. Marks, B. M. Preedom, R. L. Burman, M. A. Moinester, R. P. Redwine, F. E. Bertrand, T. P. Cleary, E. E. Gross, C. A. Ludemann, and K. Gotow, Phys. Rev. C 17, 1395 (1978).
[14]H. Dollard, K. L. Erdman, R. R. Johnson, M. R. Johnston, T. Masterson, and P. Walden, Phys. Lett. 63B, 416 (1976); R. R. Johnson, T. Masterson, K. L. Erdman, A. W. Thomas, and R. H. Landau, Nucl. Phys. A296, 444 (1978).
[15]S. A. Dytman, J. F. Amann, P. D. Barnes, J. N. Craig, K. G. R. Doss, R. A. Eisenstein, J. D. Sherman, W. R. Wharton, G. R. Burleson, S. L. Verbeck, R. J. Peterson, and H. A. Thiessen, Phys. Rev. Lett. 38, 1059 (1977); 39, 53 (1977).
[16]J. F. Amann, P. D. Barnes, K. G. R. Doss, S. A. Dytman, R. A. Eisenstein, and A. C. Thompson, Phys. Rev. Lett. 35, 426 (1975).
[17]M. D. Cooper and R. A. Eisenstein, Phys. Rev. C 13, 1334 (1976).
[18]R. Landau, S. Phatak, and F. Tabakin, Ann. Phys. (N.Y.) 78, 299 (1973).
[19]G. A. Miller, Phys. Rev. C 10, 1242 (1974) and references cited therein. S. Phatak, Ph.D. thesis, University of Pittsburgh, 1974 (unpublished). See also L. Heller, in *Meson-Nuclear Physics*—1976, proceedings of the International Topical Conference, Pittsburgh, edited by P. D. Barnes, R. A. Eisenstein, and L. S. Kisslinger (AIP, New York, 1976), p. 93.
[20]M. Sternheim and R. Silbar, Annu. Rev. Nucl. Sci. 24, 249 (1974).
[21]J. Hufner, Phys. Rep. 21C, 1 (1975).
[22]D. S. Koltun, Adv. Nucl. Phys. 3, 71 (1969).
[23]R. H. Landau and A. W. Thomas, Phys. Lett. 61B, 361 (1976); report, 1977 (unpublished).
[24]N. J. DiGiacomo, A. S. Rosenthal, E. Rost, and D. Sparrow, Phys. Lett. 66B, 421 (1977).
[25]L. C. Liu and C. Shakin, Phys. Rev. C 16, 333 (1977); 16, 1963 (1977); L. Celenza, L. C. Liu, and C. Shakin, *ibid.* 11, 1593 (1975); L. C. Liu, report (unpublished); L. C. Liu and C. Shakin, report, 1978 (unpublished).
[26]K. Stricker, H. McManus, and J. Carr, report, 1977 (unpublished).
[27]G. Fäldt, Nucl. Phys. A206, 176 (1973); Phys. Rev. C 5, 400 (1972).
[28]G. A. Miller, Nucl. Phys. A224, 269 (1974).
[29]Kwang-Bock Yoo and M. Sternheim, Phys. Rev. Lett. 40, 498 (1978).
[30]M. D. Cooper and R. A. Eisenstein, Los Alamos Report No. LA-5929-MS (unpublished).
[31]C. W. deJager, H. DeVries, and C. DeVries, At. Data Nucl. Data Tables 14, 479 (1974).
[32]G. Rowe, M. Salomon, and R. Landau, see Ref. 1 (contribution); also "CERN THEORY" from Lawrence Radiation Laboratory Report No. UCRL-20030 πN, (1970) (unpublished); L. D. Roper, L. D. Wright, and B. T. Feld, Phys. Rev. 138, B190 (1965).
[33]M. Krell and T. E. O. Ericson, Nucl. Phys. B11, 521 (1969).
[34]W. R. Gibbs, B. F. Gibson, and G. J. Stephenson, Jr., Los Alamos Report No. LA-UR-77-2136 (unpublished).
[35]G. A. Miller, Phys. Rev. C 14, 2230 (1976); 16, 2325 (1977); Phys. Rev. Lett. 38, 753 (1977).
[36]L. S. Kisslinger and W. Wang, Ann. Phys. (N.Y.) 99, 374 (1976).
[37]M. Thies, Phys. Lett. 63B, 43 (1976).
[38]R. A. Eisenstein and G. A. Miller, Comput. Phys. Commun. 11, 95 (1976).
[39]D. A. Sparrow and W. J. Gerace, Phys. Rev. Lett. 41, 1101 (1978).
[40]R. A. Eisenstein, see Ref. 1, p. 95.
[41]O. Aspelund, G. Hrehuss, A. Kiss, K. T. Knöpfle, C. Mayer-Böricke, M. Rogge, U. Schwinn, A. Seres, and P. Turek, Nucl. Phys. A253, 263 (1975).
[42]P. H. Stelson and L. Grodzins, At. Data Nucl. Data Tables 1, 29 (1965).